Microelectronic Engineering 300 (2025) 112372

Contents lists available at ScienceDirect

Microelectronic Engineering

journal homepage: www.elsevier.com/locate/mee

Research paper

Field-free magnetization switching in SOT-MRAM devices with noncollinear antiferromagnets☆

Bernhard Pruckner [a,*], Nils Petter Jørstad [a], Wolfgang Goes [c], Siegfried Selberherr [b], Viktor Sverdlov [b]

[a] Christian Doppler Laboratory for Nonvolatile Magnetoresistive Memory and Logic, Austria
[b] Institute for Microelectronics, TU Wien, Gußhausstraße 27-29/E360, 1040 Vienna, Austria
[c] Silvaco Europe Ltd. Cambridge, United Kingdom

ARTICLE INFO

Keywords:
Spintronics
SOT-MRAM
Magnetic spin hall effect
Field-free switching
Antiferromagnets

ABSTRACT

Spin-orbit torque magnetoresistive random access memory (SOT-MRAM) is a promising nonvolatile memory technology that offers fast writing speed, low power, and long endurance. However, achieving deterministic perpendicular magnetization switching typically requires an external field, limiting scalability. This work explores the incorporation of noncollinear antiferromagnetic (nc-AFMs), exhibiting the magnetic spin Hall effect (MSHE), and exchange bias to enable field-free deterministic switching. MSHE has been observed in Mn_3Sn, $MnPd_3$. The ratio of out-of-plane to in-plane polarized spin-currents is crucial for field-free MSHE-driven magnetization switching. It was found that a minimum ratio is needed to drive field-free perpendicular switching. Exchange bias acting at the interface between in-plane AFM and out-of-plane ferromagnet (FM) has been demonstrated to enable field-free SOT-driven magnetization switching. We show, that exchange bias can facilitate field-free perpendicular switching in cases of a missing or too small out-of-plane polarized spin current component. We present a fully three-dimensional finite element model that couples spin currents and magnetization dynamics to simulate SOT-MRAM devices utilizing the MSHE. We show that the use of nc-AFMs eliminates the need for external fields without compromising performance, simplifying design, and boosting scalability.

1. Introduction

Magnetoresistive random access memory (MRAM) is a nonvolatile memory technology, promising nanosecond switching times, high endurance, and high energy efficiency [1], with the potential to replace flash memory, DRAM, and even SRAM in cache memory [2–4]. The state of the cell is stored through the relative orientation of the magnetization of a perpendicularly magnetized FM free layer (FL) and a fixed reference layer (RL) within a perpendicular magnetic tunnel junction (pMTJ). SOT-MRAM have been shown to provide an effective approach to manipulate the magnetization of an FL with sub-ns switching speeds [5–9]. However, to achieve full perpendicular magnetization reversal, typically an additional external field is required, which is detrimental to the density of SOT-MRAM devices.

The current-induced spin torque acting on the magnetization can be decomposed into two orthogonal contributions with the directions $\hat{\mathbf{d}} = \widehat{\mathbf{m}} \times (\hat{\mathbf{p}} \times \widehat{\mathbf{m}})$ and $\hat{\mathbf{f}} = \hat{\mathbf{p}} \times \widehat{\mathbf{m}}$ referred to as the damping-like and field-like torque, respectively. $\hat{\mathbf{p}}$ is the polarization direction of the spin current injected into the FM and $\widehat{\mathbf{m}}$ is the local magnetic moment. Typically in SOT-MRAM based on heavy metal (HM) layers with the SHE $\hat{\mathbf{p}} = \hat{\mathbf{n}} \times \hat{\mathbf{E}}$, where $\hat{\mathbf{n}}$ is the interface normal of the HM/FM interface and $\hat{\mathbf{E}}$ is the direction of the applied electric field.

The generation of additional out-of-plane spin-polarized spin currents, necessary for field-free switching, has been observed in multilayer structures incorporating nc-AFMs, specifically in an Mn_3Sn/Cu/FM trilayer [10] and $MnPd_3$/FM bilayer [11]. Additionally field-free switching has been achieved by the exchange bias induced by an AFM like PtMn or IrMn at the FM/AFM interface [12,13].

Fig. 1 illustrates the arrangement of the Sn and Mn atoms, where the magnetic moments are depicted. The three magnetic sublattices $\mathbf{m_A}$, $\mathbf{m_B}$

☆ This article is part of a Special issue entitled: 'AMNDCE' published in Microelectronic Engineering.

* Corresponding author.
E-mail address: pruckner@iue.tuwien.ac.at (B. Pruckner).

https://doi.org/10.1016/j.mee.2025.112372
Received 31 January 2025; Received in revised form 18 May 2025; Accepted 3 June 2025
Available online 8 June 2025

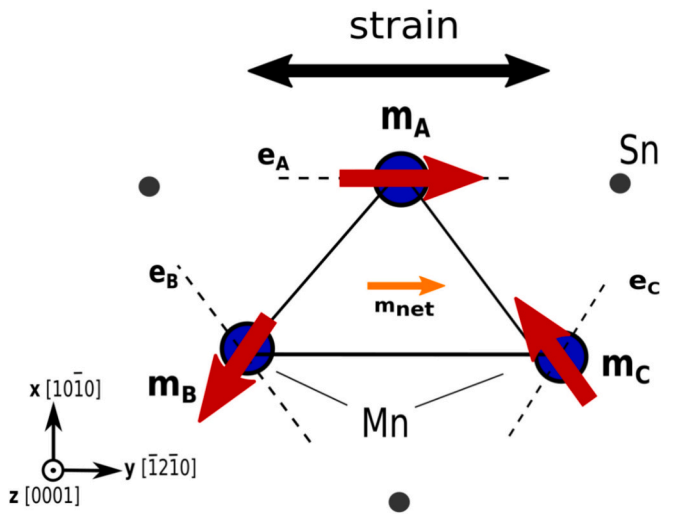

Fig. 1. Sketch for the crystal and magnetic structure of the Mn_3Sn nc-AFM. Blue and dark grey spheres represent Mn and Sn atoms, respectively. The red arrows represent the magnetic moments of Mn atoms. The black dashed lines represent the magnetic easy axes of individual sublattice moments. Strain is applied along x-direction. The orange arrow represents the small net-magnetic moment. (For interpretation of the references to colour in this figure legend, the reader is referred to the web version of this article.)

and $\mathbf{m_C}$ of the nc-AFMs are arranged in a triangular shape within a two-dimensional kagome lattice in the xz-plane [14]. The magnetic moments are coupled via antiferromagnetic exchange, and each magnetic moment exhibits an individual magnetic anisotropy along the easy axes designated as $\mathbf{e_A}$, $\mathbf{e_B}$ and $\mathbf{e_C}$. In an unstrained state, the magnetic moments of the sublattices cancel out and the net magnetization m_{net} is zero.

Introducing epitaxial tensile strain into the crystal lattice along the x-direction ([$\bar{1}$2$\bar{1}$0]-direction) modulates the exchange interaction and the magnetic anisotropy leading to a small nonvanishing net-magnetization $m_{net} > 0$, as the magnetic moments of the sublattices do not fully cancel out each other. The magnetic configuration in the strained Mn_3Sn exhibits four stable states, two with the net-magnetization pointing along the positive or negative x-direction (AFM1, displayed in Fig. 1) and two with the net-magnetization along positive or negative z-direction (AFM2) [10,15]. The states of Mn_3Sn with the net-magnetization in perpendicular as well as in-plane direction can both facilitate the generation of out-of-plane spin-polarized spin currents. In this work we focus on the AFM1 state which can facilitate field-free switching with a charge current applied along x-direction [10].

The AFM in the Mn_3Sn/Cu/FM trilayer structure is separated by a nonmagnetic Cu spacer layer, to magnetically decouple the AFM and FM layers and ensure the switching process is solely driven by MSHE-generated spin currents.

In Section 2 we describe the micromagnetic model utilized in our micromagnetics simulation framework ViennaSpinMag [16,17]. The finite element method (FEM) is employed for the numerical simulation of the magnetization dynamics, utilizing the Landau-Lifshitz-Gilbert (LLG) equation, and in Section 3 we describe our coupled spin and charge drift-diffusion model used to describe spin currents arising in SOT-MRAM devices. In Section 4 we investigate the distinct spin torques in AFM/FM bilayer structures and analyze the damping-like and field-like torque contributions. In Section 5 we investigate the performance of three distinct SOT-MRAM devices, shown in Fig. 2, utilizing (a) the SHE and interfacial Rashba-Edelstein effect in a Pt HM layer [18], (b) the MSHE in an Mn_3Sn layer, and (c) the MSHE in an $MnPd_3$ layer as well as exchange bias at the AFM/FM interface.

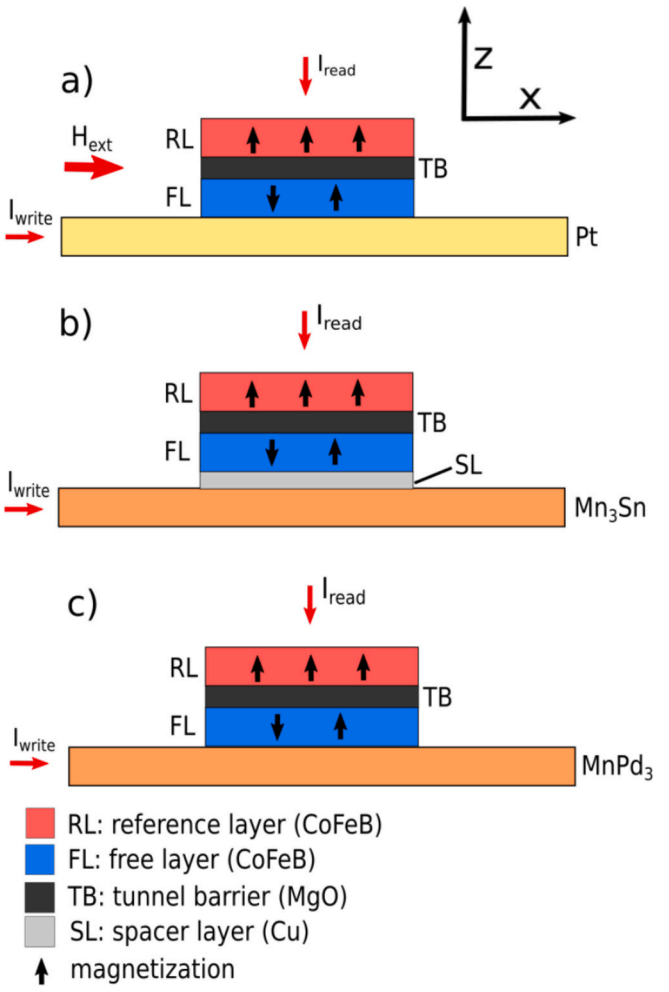

Fig. 2. Three distinct SOT-MRAM cells, consisting of a CoFeB(1 nm)/MgO(1 nm)/CoFeB(1 nm) pMTJ placed on top of (a) a Pt(4 nm) layer, (b) an Mn_3Sn(7 nm) layer with a Cu(1 nm) nonmagnetic spacer layer for magnetic decoupling of the AFM and FL, and (c) an $MnPd_3$(7 nm) layer. A charge current is applied in x-direction. An additional external magnetic field of 60 mT is applied in x-direction in a). The magnetization of the ferromagnetic CoFeB layers is indicated with black arrows.

2. Micromagnetic model

To model the current-induced magnetization dynamics in SOT-MRAM we utilize the micromagnetic LLG equation, with an additional term that describes the spin torques [19]:

$$\frac{\partial \mathbf{m}}{\partial t} = -\gamma_0 \mathbf{m} \times \mathbf{H_{eff}} + \alpha \mathbf{m} \times \frac{\partial \mathbf{m}}{\partial t} + \frac{1}{M_S}\mathbf{T_S} \tag{1}$$

The LLG describes the precession and damping of the normalized local magnetization $\mathbf{m} = \mathbf{M}/M_S$ towards an effective field $\mathbf{H_{eff}}$, where M_S is the saturation magnetization. $\mathbf{T_S}$ describes the local spin torques acting on the magnetization. $\gamma_0 = -\gamma\mu_0$ is the rescaled gyromagnetic ratio, where μ_0 is the permeability of vacuum, and α is the dimensionless Gilbert damping constant. The effective field contains the contributions from the ferromagnetic exchange, the perpendicular magnetic anisotropy, the demagnetizing field, and the exchange basis at the AFM/FM interface. The demagnetizing field is computed through a hybrid FEM-Boundary Element Method (FEM-BEM) approach [20].

In order to capture the local variation of the spin polarization we express the torques arising from the nonequilibrium spin density **S**. The spin torques are then obtained from the loss of transversely polarized spin current in the FM layers, due to the conservation of angular mo-

mentum [16,21]:

$$\mathbf{T_S} = -\frac{D_e}{\lambda_J^2}\mathbf{m}\times\mathbf{S} - \frac{D_e}{\lambda_\varphi^2}\mathbf{m}\times(\mathbf{m}\times\mathbf{S}) \tag{2}$$

D_e is the electron diffusion coefficient, λ_J is the exchange length,and λ_φ is the spin dephasing length of the FM.

The spins of the AFM are locked, and those adjacent to the AFM/FM interface act to keep the spins in the FM on the other side in the same direction through exchange coupling. The system behaves as if an effective field is present, which breaks the inversion symmetry and can facilitate deterministic switching, similar to an externally applied magnetic field [13,22]. The effective bias field H_{eb} is given by

$$H_{eb} = -\frac{J_{eb}}{\mu_0 M_S t_{FM}}. \tag{3}$$

J_{eb} is the interfacial exchange energy density, and t_{FM} is the thickness of the FM layer. H_{eb} can be determined by hysteresis measurements, where it acts like an applied external field, that shifts the hysteresis loop.

3. Spin drift-diffusion model

In order to calculate the torques acting on the FM layers, the charge and spin transport in the structures have to be evaluated. The nonequilibrium spin accumulation is obtained from its continuity equation:

$$\frac{\partial\mathbf{S}}{\partial t} = 0 = -\nabla\cdot\overline{\mathbf{J_S}} - D_e\left(\frac{\mathbf{S}}{\lambda_{sf}^2} + \frac{\mathbf{S}\times\mathbf{m}}{\lambda_J^2} + \frac{\mathbf{m}\times(\mathbf{S}\times\mathbf{m})}{\lambda_\varphi^2}\right) \tag{4}$$

It can be assumed that the spin immediately adapts to the changes in magnetization as its dynamics typically are three orders of magnitude faster [23]. Therefore, the equation is solved for its steady state. $(\overline{\mathbf{J_S}})_{ij}$ is the spin polarization current density in units of A/s, where i is the polarization component and j is the current direction. λ_{sf} is the spin-flip length. We express the spin polarization current density in terms of the charge current density [16]:

$$\overline{\mathbf{J_S}} = -\frac{\mu_B}{e}\beta_\sigma\mathbf{m}\otimes\left(\mathbf{J_C} - \beta_D D_e\frac{e}{\mu_B}\left[(\nabla\mathbf{S})^{\mathrm{T}}\mathbf{m}\right]\right) - D_e\nabla\mathbf{S} \tag{5}$$

μ_B is the Bohr magneton and e is the elementary charge. β_σ is the charge current spin polarization and β_D is the diffusion spin polarization. $\otimes$ denotes the outer product between two vectors, and $(\cdot)^{\mathrm{T}}$ is the matrix transpose. The charge current density from an applied field is obtained from Ohms law $\mathbf{J_C} = \sigma\mathbf{E}$, where σ is the electrical conductivity, and $\mathbf{E}$ is the electric field. Using the relations $\mathbf{E} = -\nabla V$ and $\nabla\cdot\mathbf{J_C} = 0$, we obtain the following Poisson equation for the electrical potential:

$$\nabla\cdot(-\sigma\nabla V) = 0 \tag{6}$$

The equation is solved using Dirichlet boundary conditions for the applied voltage at the contacts and zero flux boundary conditions at boundaries not containing contacts.

In the SOT-MRAM devices, spin current is generated in an HM or nc-AFM layer. It flows perpendicularly to the applied charge current. In general, the spin current can be described by:

$$\overline{\mathbf{J_S}}_{,SOT} = -\frac{\mu_B}{e}\overline{\theta}_{SCA}\mathbf{J_C} \tag{7}$$

with

$$\overline{\theta}_{SCA} = \overline{\sigma}_{\mathbf{SH}}\rho \tag{8}$$

$\overline{\theta}_{SCA}$ is the spin-charge angle (SCA) tensor and describes the charge-to-spin conversion [24]. The SCA tensor is a generalization of the scalar spin Hall angle, used to describe the charge-to-spin conversion by the conventional SHE. $\overline{\sigma}_{\mathbf{SH}}$ is the spin Hall conductivity tensor (SHCT) and ρ is the electric resistivity. In the case of the conventional SHE, the SHCT is described by:

$$\sigma^{\mathbf{S_k}}_{\mathbf{SH},\mathbf{ij}} = \epsilon_{\mathbf{ijk}}\sigma_{SH}. \tag{9}$$

ϵ_{ijk} is the Levi-Civita tensor and σ_{SH} is the spin-Hall conductivity, which is a single isotropic quantity related to the spin-Hall angle by $\theta_{SHA} = \sigma_{SH}\cdot\rho$ [24]. In the case of the SHE, the nonzero components of the SHCT only generate in-plane spin-polarized spin currents, if the charge current flows parallel to the FM-HM interface. The spin current generated by the SHE with a charge current applied along x-direction can be written as follows:

$$\overline{\mathbf{J}}_{\mathbf{S}SHE} = \frac{-\mu_B}{e}\left(\begin{bmatrix}0 & 0 & 0\\ 0 & 0 & \sigma_{SH}\\ 0 & -\sigma_{SH} & 0\end{bmatrix}\rho\right)J_{C,x} \tag{10}$$

In the MSHE, additional nonzero components of the SHCT generate out-of-plane spin-polarized spin currents. The magnetic spin Hall conductivity tensors (MSHCT) $\sigma^{S_k}_{MSH}$ describing the MSHE in the AFM1 and AFM2 state of Mn_3Sn respectively, are written as follows [10,24]:

$$\begin{array}{lll} & \sigma^{S_k}_{MSH|AFM1} & \sigma^{S_k}_{MSH|AFM2}\\ \sigma^{S_x}_{MSH}: & \begin{bmatrix}0 & 0 & 0\\ 0 & \sigma^x_{yy} & 0\\ 0 & 0 & -\sigma^x_{zz}\end{bmatrix} & \begin{bmatrix}0 & \sigma^x_{xy} & 0\\ -\sigma^x_{yx} & 0 & 0\\ 0 & 0 & 0\end{bmatrix}\\ \sigma^{S_y}_{MSH}: & \begin{bmatrix}0 & \sigma^y_{xy} & 0\\ -\sigma^y_{yx} & 0 & 0\\ 0 & 0 & 0\end{bmatrix} & \begin{bmatrix}0 & 0 & 0\\ 0 & \sigma^y_{yy} & 0\\ 0 & 0 & -\sigma^y_{zz}\end{bmatrix}\\ \sigma^{S_z}_{MSH}: & \begin{bmatrix}0 & 0 & -\sigma^z_{xz}\\ 0 & 0 & 0\\ \sigma^y_{zx} & 0 & 0\end{bmatrix} & \begin{bmatrix}0 & 0 & 0\\ 0 & 0 & \sigma^z_{yz}\\ 0 & -\sigma^z_{zy} & 0\end{bmatrix}\end{array} \tag{11}$$

The columns and rows of the σ_{MSH} matrices represent the direction and the spin-polarization of the spin current respectively. Thus the zz-component of the $\sigma^{S_x}_{MSH|AFM1}$-matrix produces a z-polarized spin current in z-direction, when a charge current along x-direction is applied. Therefore we focus on Mn_3Sn in the AFM1 state, to investigate the generation of out-of-plane spin current. In nc-AFMs spin current is generated by the SHE and the MSHE. The total spin current generated by a charge current applied in x-direction can be expressed as follows:

$$\overline{\mathbf{J_S}} = \overline{\mathbf{J}}_{\mathbf{S}SHE} + \frac{-\mu_B}{e}\left(\begin{bmatrix}0 & 0 & 0\\ 0 & \sigma^x_{MSH,yy} & 0\\ 0 & 0 & -\sigma^x_{MSH,zz}\end{bmatrix}\rho\right)J_{C,x} \tag{12}$$

At boundaries between nonmagnetic and FM layers, we use the boundary conditions from the magnetoelectronic circuit theory [21,25], where the currents are related to the charge and spin potential drops across the interface through interface conductances:

$$\mathbf{J_C}\cdot\mathbf{n} = (G^\uparrow + G^\downarrow)\Delta V - (G^\uparrow - G^\downarrow)\Delta\mathbf{V_S}\cdot\mathbf{m} \tag{13}$$

$$\begin{aligned}\mathbf{J_S}\mathbf{n} = \frac{\mu_B}{e}\big[&2\ \mathrm{Re}[G^{\uparrow\downarrow}]\mathbf{m}\times(\mathbf{m}\times\Delta\mathbf{V_S})\\ &+2\ \mathrm{Im}[G^{\uparrow\downarrow}]\mathbf{m}\times\Delta\mathbf{V_S}\\ &-(G^\uparrow + G^\downarrow)(\Delta\mathbf{V_S}\cdot\mathbf{m})\mathbf{m} + (G^\uparrow - G^\downarrow)\Delta V\mathbf{m}\big]\end{aligned} \tag{14}$$

$G^\uparrow(G^\downarrow)$ is the interface conductance of the majority (minority) electrons, while $G^{\uparrow\downarrow}$ is the complex interface spin mixing conductance. The spin chemical potential is proportional to the spin accumulation $\mathbf{V_S} = \frac{e}{\mu_B}\frac{D_e}{\sigma}\mathbf{S}$.

4. Spin-torques

We consider an Mn_3Sn(5 nm)/CoFeB(1 nm) and an $MnPd_3$(5 nm)/CoFeB(1 nm) bilayer structure with an applied in-plane electric current density of $5*10^{11}$ A/m^2. Both, Mn_3Sn and $MnPd_3$, exhibit the MSHE with reported SCAs of $\theta_{SCA,x} = 0.0$, $\theta_{SCA,y} = 0.22$, $\theta_{SCA,z} = 0.063$ and $\theta_{SCA,x} = 0.017$, $\theta_{SCA,y} = 0.41$, $\theta_{SCA,z} = 0.011$ respectively [10,11], with $\theta_{SCA,i} = \sigma_{SH,i}\rho$ [24]. We describe the CoFeB magnetization direction in terms of the azimuthal and polar angle $m = [\cos(\phi)\sin(\theta), \sin(\phi)\sin(\theta), \cos(\theta)]$, such that for $\theta = 90^\circ$ and $\phi = 0^\circ$ it points along the direction of the current and out-of-plane for $\theta = 0^\circ$. We solve the drift-diffusion equations for the bilayer systems and analyze the angular dependence of the torques. The angular dependence of the structure's torque is depicted in Fig. 3. The minimum of the plot corresponds to the spin current polarization direction $\hat{\boldsymbol{p}}$, along which the magnetization will align when a high enough current is applied to surpass the energy barrier of the magnetic anisotropy. When the current is switched off the magnetization will relax to either $+\hat{\mathbf{z}}$ or $-\hat{\mathbf{z}}$ depending on how close $\hat{\boldsymbol{p}}$ is to either and which current independent fields are present. Typically the SHE $\hat{\boldsymbol{p}}$ points in-plane, meaning that the magnetization has no preferred direction to relax towards, leading to a nondeterministic switching process. A $\hat{\boldsymbol{p}}$ pointing slightly out-of-plane, which is more pronounced in Mn_3Sn, shown in Fig. 3a) than in $MnPd_3$ shown in Fig. 3b), indicates that the spin torques produced by the MSHE can facilitate deterministic out-of-plane switching.

By extracting $\hat{\boldsymbol{p}}$ from Fig. 3 and projecting the torque along $\hat{\mathbf{d}}$ and $\hat{\mathbf{f}}$ we obtain the damping-like and field-like components of the torque. Fig. 4 shows the dependence of the a) damping-like and b) field-like spin torque on the thickness of the Mn_3Sn and $MnPd_3$ layers. The damping- and field-like components both increase with the AFM thickness until reaching a saturation point, depending on the spin-diffusion length of the material. With decreasing AFM thickness both spin-torque components vanish, showing the nature of the MSHE as a bulk effect.

5. Switching performance

We consider the SHE-driven devices depicted in Fig. 2a) with an applied external magnetic field and the MSHE-driven device depicted in Fig. 2b). We apply our combined drift-diffusion and micromagnetic model to the SOT-devices and analyze the switching performance from the anti-parallel (ap) state, with the magnetization of free layer and reference layer in negative and positive z-direction, respectively, to the parallel (p) state, with the magnetization of both FM layers in positive z-direction.

A positive charge current pulse is applied to the Mn_3Sn and Pt layers in x-direction. Switching times for the Mn_3Sn-based devices were compared to conventional SHE switching in a Pt-based SOT-MRAM cell with an external field $H_{ex} = 60$ mT, as shown in Fig. 5. MSHE-driven field-free perpendicular switching is competitive with SHE switching, achieving sub-nanosecond switching times, at current densities exceeding $7*10^{12}$ A/m^2.

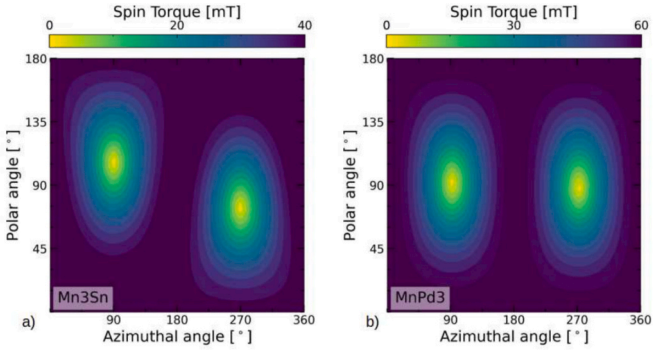

Fig. 3. Angular dependence of the spin torque acting on the magnetization of the FM in an AFM(5 nm)/CoFeB(1 nm) bilayer. The spin torque is depicted for (a) Mn_3Sn and (b) $MnPd_3$. A current of $5*10^{11}$ A/m^2 is applied along x.

We perform the same switching simulations for the $MnPd_3$-based device shown in Fig. 2c). No perpendicular magnetization switching could be achieved in the $MnPd_3$-based device by only considering the MSHE. After the magnetization of the FL was driven in-plane, no out-of-plane motion of the magnetization was observed. The ratio of conventional and unconventional SHCT components $R_\sigma = \sigma^z/\sigma^y$ in $MnPd_3$ is $R_{\sigma,MnPd3} = 0.026$, which is much smaller than in Mn_3Sn with $R_{\sigma Mn3Sn} = 0.3$. We analyze the significance of R_σ for the performance of MSHE-driven perpendicular switching. The inset in Fig. 5 depicts the switching time for MSHE-driven field-free magnetization switching for different R_σ for current densities of 5, 7.5 and $10*10^{12}$ A/m^2. The minimal ratio to achieve switching was $R_\sigma = 0.1$ for a current density of $j_c = 1.0*10^{13}$, $R_\sigma = 0.2$ for $j_c = 7.5*10^{12}$, and $R_\sigma = 0.24$ for $j_c = 5.0*10^{12}$.

In order to further investigate the impact of the SHCT-ratio $R_\sigma = \sigma_z/\sigma_y$ on the switching performance, we conduct a series of switching simulations of an MSHE-driven device, to explore the optimal switching performance as well as the minimum value of R_σ necessary for field-free MSHE-driven magnetization switching. Fig. 6 illustrates the switching time for various combinations of SHCT-ratio and current density j_C. Below a value of $R_\sigma = 0.1$ no magnetization switching was achieved, even for current densities $j_C > 1*10^{13} A/m^2$. While it may seem intuitive that higher currents can drive switching for even lower SHCT-ratios, the in-plane torques generated by the in-plane spin current components become strong enough to keep the magnetization in-plane and therefore preventing perpendicular switching. $R_\sigma = 0.1$ is the minimal cut off value for perpendicular MSHE-driven magnetization switching. Contrarily, the switching performance increased for high SHCT-ratios. Magnetization switching in an $MnPd_3$/CoFeB bilayer is likely not solely caused by the MSHE, as the SCHT-ratio of $MnPd_3$ of $R_{\sigma,MnPd3} = 0.026$ lies below the minimal threshold value observed in our simulations. The presence of interfacial effects like exchange bias, likely facilitates deterministic field-free magnetization switching in the $MnPd_3$-based device.

Fig. 7 shows the z-component of the normalized magnetization for an SOT device with an $MnPd_3$ layer, for several interfacial exchange energy densities J_{eb}. J_{eb} is typically in the order of 10^{-3} J/m^2, depending on the annealing of the AFM layer [22,26]. Without exchange bias ($J_{eb} = 0$), the magnetization is driven in-plane, as the out-of-plane spin currents generated in $MnPd_3$ are not enough to push the magnetization sfurther towards the $-z$-direction. If exchange bias is applied ($J_{eb} > 0$), the effective exchange bias field H_{eb} acts similar to an applied external field and helps to complete the perpendicular magnetization switching. An out-of-plane magnetization can be observed. Large enough J_{eb} enable fully field-free perpendicular magnetization switching, emphasizing the importance of the interface exchange bias in SOT-MRAM devices incorporating AFM materials.

6. Conclusion

We employ a fully three-dimensional FEM-based simulation approach to evaluate the switching performance of SOT-MRAM devices. We extend the conventional SHE-driven MRAM structure by incorporating the nc-AFMs Mn_3Sn and $MnPd_3$, which exhibit the MSHE. We introduce the experimentally reported generation of out-of-plane spin-polarized spin current by the MSHE in our model. The non-conventional spin current components generate torques, that can facilitate field-free perpendicular magnetization switching of an adjacent FM. The switching performance depends on the ratio of conventional to non-conventional SHCT components $R_\sigma = \sigma^z/\sigma^y$ and the current density. While the ratio of $R = 0.3$ in Mn_3Sn is sufficient to enable purely MSHE-

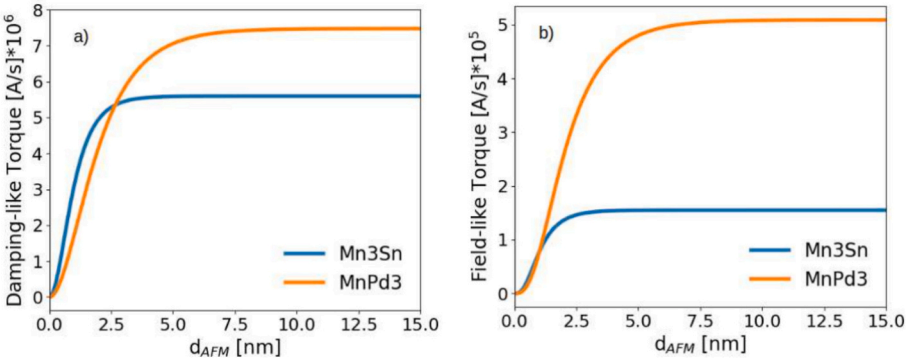

Fig. 4. Thickness dependence of the (a) damping-like and (b) field-like spin torque acting on the magnetization of the FM in an AFM(d_{AFM})/CoFeB(1 nm) bilayer structure, with Mn_3Sn and $MnPd_3$ as AFM materials. A current of $5*10^{11}$ A/m^2 is applied along x.

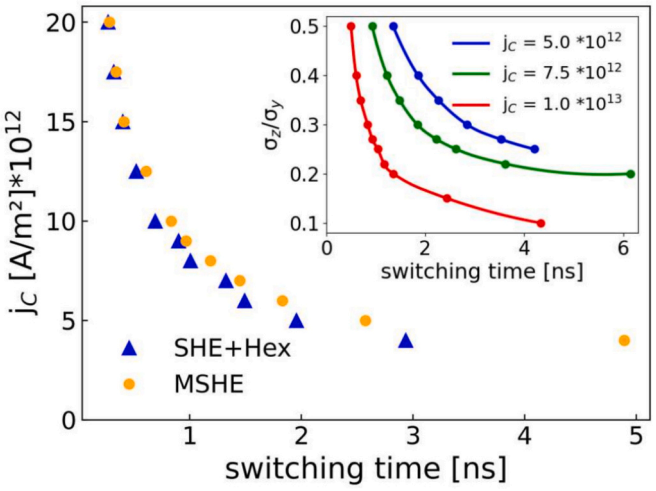

Fig. 5. Switching performance of the SOT devices shown in Fig. 2a) and b). The inset shows the switching time for MSHE-driven field-free perpendicular magnetization switching for several conventional to unconventional SHCT component ratios, for applied current densities j_C of 5, 7.5 and $10*10^{12}A/m^2$.

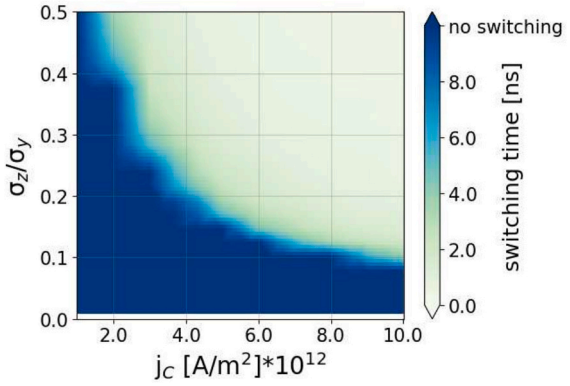

Fig. 6. Switching time for different applied current densities j_C and SHCT-ratios σ_z/σ_y. A 10 ns charge current pulse was applied to an MSHE-driven SOT-device.

driven field-free switching, $MnPd_3$ with $R = 0.026$ does not exhibit field-free perpendicular switching solely driven by the MSHE. We determine a minimal SHCT-ratio of $R_\sigma = 0.1$ to enable field-free magnetization switching solely driven by the MSHE. By considering also the exchange bias at the AFM/FM interface, the $MnPd_3$-based device exhibits field-free perpendicular magnetization switching, delivering a possible explanation for the experimentally observed switching in $MnPd_3$/FM bilayers [11] and the enhancement of the switching performance of MSHE-driven SOT-devices.

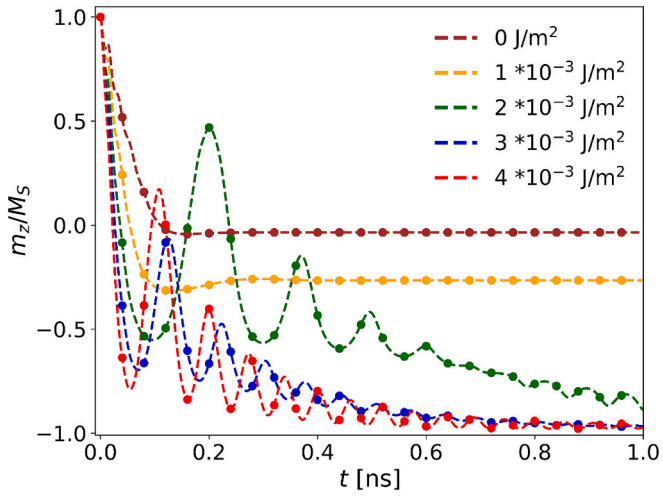

Fig. 7. The normalized z-component of the magnetization in the FL of the device depicted in Fig. 2c), for different interfacial exchange energy densities J_{eb}. A charge current density of $j_C = 3*10^{12}$ A/m^2 is applied along x-direction.

CRediT authorship contribution statement

Bernhard Pruckner: Conceptualization, Methodology, Investigation, Software, Visualization, Writing – original draft. **Nils Petter Jørstad:** Software, Writing – review & editing, Visualization. **Wolfgang Goes:** Writing – review & editing. **Siegfried Selberherr:** Writing – review & editing. **Viktor Sverdlov:** Conceptualization, Supervision, Writing – review & editing, Funding acquisition.

Declaration of competing interest

The authors declare that they have no known competing financial interests or personal relationships that could have appeared to influence the work reported in this paper.

Acknowledgments

The financial support by the Federal Ministry for Economy, Energy and Tourism, and the National Foundation for Research, Technology and Development, and the Christian Doppler Research Association is gratefully acknowledged. The authors acknowledge TU Wien Bibliothek for financial support through its Open Access Funding Program.

Data availability

Data will be made available on request.

References

[1] T.Y. Lee, J.M. Lee, M.K. Kim, J.S. Oh, J.W. Lee, H.M. Jeong, P.H. Jang, M.K. Joo, K. Suh, S.H. Han, D.-E. Jeong, T. Kai, J.H. Jeong, J.-H. Park, J.H. Lee, Y.H. Park, E. B. Chang, Y.K. Park, H.J. Shin, Y.S. Ji, S.H. Hwang, K.T. Nam, B.S. Kwon, M.K. Cho, B.Y. Seo, Y.J. Song, G.H. Koh, K. Lee, J.-H. Lee, G.T. Jeong, World-most energy-efficient mram technology for non-volatile RAM applications, in: International Electron Devices Meeting (IEDM), 2022, pp. 10.7.1–10.7.4.

[2] R. Saha, Y.P. Pundir, P. Kumar Pal, Comparative analysis of STT and SOT based MRAMs for last level caches, J. Magn. Magn. Mater. 551 (2022) 169161.

[3] F. Oboril, R. Bishnoi, M. Ebrahimi, M.B. Tahoori, Evaluation of hybrid memory technologies using SOT-MRAM for on-Chip cache hierarchy, IEEE Trans. Comp. Aid. Design Integrat. Circuits Syst. 34 (3) (2015) 367–380.

[4] Q. Shao, P. Li, L. Liu, H. Yang, S. Fukami, A. Razavi, H. Wu, K. Wang, F. Freimuth, Y. Mokrousov, M.D. Stiles, S. Emori, A. Hoffmann, J. Åkerman, K. Roy, J.-P. Wang, S.-H. Yang, K. Garello, W. Zhang, Roadmap of Spin–Orbit Torques, IEEE Trans. Magn. 57 (7) (2021) 1–39.

[5] X. Qiu, Z. Shi, W. Fan, S. Zhou, H. Yang, Characterization and manipulation of spin orbit torque in magnetic heterostructures, Science 336 (6081) (2012) 555–558.

[6] I. Mihai Miron, G. Gaudin, S. Auffret, B. Rodmacq, A. Schuhl, S. Pizzini, J. Vogel, P. Gambardella, Current-driven spin torque induced by the Rashba effect in a ferromagnetic metal layer, Nat. Mater. 9 (3) (2010) 230–234.

[7] L. Liu, O.J. Lee, T.J. Gudmundsen, D.C. Ralph, R.A. Buhrman, Current-induced switching of perpendicularly magnetized magnetic layers using spin torque from the spin hall effect, Phys. Rev. Lett. 109 (2012) 096602.

[8] L. Liu, C.-F. Pai, Y. Li, H.W. Tseng, D.C. Ralph, R.A. Buhrman, Spin-torque switching with the Giant spin hall effect of tantalum, Science 336 (6081) (2012) 555–558.

[9] I.M. Miron, K. Garello, G. Gaudin, P.-J. Zermatten, M.V. Costache, S. Auffret, S. Bandiera, B. Rodmacq, A. Schuhl, P. Gambardella, Perpendicular switching of a single ferromagnetic layer induced by in-plane current injection, Nature 476 (7359) (2011) 189–193.

[10] S. Hu, D.-F. Shao, H. Yang, C. Pan, Z. Fu, M. Tang, Y. Yang, W. Fan, S. Zhou, E. Y. Tsymbal, X. Qiu, Efficient perpendicular magnetization switching by a magnetic spin hall effect in a noncollinear antiferromagnet, Nat. Commun. 13 (2022) 4447.

[11] M. DC, D.-F. Shao, V.D.-H. Hou, A. Vailionis, P. Quarterman, A. Habiboglu, M. B. Venuti, F. Xue, Y.-L. Huang, C.-M. Lee, M. Miura, B. Kirby, C. Bi, X. Li, Y. Deng, S.-J. Lin, W. Tsai, S. Eley, W.-G. Wang, J.A. Borchers, E.Y. Tsymbal, S.X. Wang, Observation of anti-damping spin–orbit torques generated by in-plane and out-of-plane spin polarizations in MnPd3, Nat. Mater. 22 (2023) 591–598.

[12] Y.-W. Oh, S.-H. Chris Baek, Y.M. Kim, H.Y. Lee, K.-D. Lee, C.-G. Yang, E.-S. Park, K.-S. Lee, K.-W. Kim, Y. Go, J.-R. Jeong, B.-C. Min, H.-W. Lee, K.-J. Lee, B.-G. Park, Field-free switching of perpendicular magnetization through spin–orbit torque in antiferromagnet/ferromagnet/oxide structures, Nat. Nanotechnol. 11 (10) (2016) 878–884.

[13] S. Fukami, C. Zhang, S. DuttaGupta, A. Kurenkov, H. Ohno, Magnetization switching by spin–orbit torque in an antiferromagnet–ferromagnet bilayer system, Nat. Mater. 15 (2016) 535–541.

[14] T. Higo, K. Kondou, T. Nomoto, M. Shiga, S. Sakamoto, X. Chen, D. Nishio-Hamane, Y. Arita, Y. Otani, S. Miwa, S. Nakatsuji, Perpendicular full switching of chiral antiferromagnetic order by current, Nature 607 (2022) 474–479.

[15] J.-Y. Yoon, P. Zhang, C.-T. Chou, Y. Takeuchi, T. Uchimura, J.T. Hou, J. Han, S. Kanai, H. Ohno, S. Fukami, L. Liu, Handedness anomaly in a non-collinear antiferromagnet under spin–orbit torque, Nat. Mater. 22 (2023) 1106–1113.

[16] S. Fiorentini, M. Bendra, J. Ender, R.L. de Orio, W. Goes, S. Selberherr, V. Sverdlov, Spin and charge drift-diffusion in ultra-scaled MRAM cells, Sci. Rep. 12 (2022) 20958.

[17] CDL NovoMemLog, ViennaSpinMag, last accessed on 30 March 2023. URL, https://www.iue.tuwien.ac.at/viennaspinmag/.

[18] N.P. Jørstad, S. Fiorentini, J. Ender, W. Goes, S. Selberherr, V. Sverdlov, Micromagnetic modeling of SOT-MRAM dynamics, Phys. B Condens. Matter 676 (2024) 415612.

[19] T.L. Gilbert, A phenomenological theory of damping in ferromagnetic materials, IEEE Trans. Magn. 40 (2004) 3443–3449.

[20] J. Ender, M. Mohamedou, S. Fiorentini, R. Orio, S. Selberherr, W. Goes, V. Sverdlov, Efficient demagnetizing field calculation for disconnected complex geometries in STT-MRAM cells, in: 2020 International Conference on Simulation of Semiconductor Processes and Devices (SISPAD), 2020, pp. 213–216.

[21] P.M. Haney, H.-W. Lee, K.-J. Lee, A. Manchon, M.D. Stiles, Current induced torques and interfacial spin-orbit coupling: semiclassical modeling, Phys. Rev. B 87 (2013) 174411.

[22] S. Alla, V. Kumar Joshi, S. Bhat, Field-free switching of VG-SOT-pMTJ device through the interplay of SOT, exchange Bias, and VCMA effects, J. Appl. Phys. 134 (2023) 013901.

[23] S. Zhang, P.M. Levy, A. Fert, Mechanisms of spin-polarized current-driven magnetization switching, Phys. Rev. Lett. 88 (2002) 236601.

[24] L. Salemi, P.M. Oppeneer, Theory of magnetic spin and orbital hall and Nernst effects in bulk ferromagnets, Phys. Rev. B 106 (2022) 024410.

[25] A. Brataas, G.E. Bauer, P.J. Kelly, Non-collinear Magnetoelectronics, Phys. Rep. 427 (2006) 157–255.

[26] K. Steenbeck, R. Mattheis, M. Diegel, Antiferromagnetic energy loss and exchange coupling of IrMn/CoFe films: experiments and simulations, J. Magn. Magn. Mater. 279 (2003) 317–324.